

# We are IntechOpen, the world's leading publisher of Open Access books Built by scientists, for scientists

6,900

Open access books available

185,000

International authors and editors

200M

Downloads

Our authors are among the

154

Countries delivered to

TOP 1%

most cited scientists

12.2%

Contributors from top 500 universities



WEB OF SCIENCE™

Selection of our books indexed in the Book Citation Index  
in Web of Science™ Core Collection (BKCI)

Interested in publishing with us?  
Contact [book.department@intechopen.com](mailto:book.department@intechopen.com)

Numbers displayed above are based on latest data collected.  
For more information visit [www.intechopen.com](http://www.intechopen.com)



# Detection of Underground Water by Using GPR

*Dalia N. Elsheakh and Esmat A. Abdallah*

## Abstract

Water is the human vital requirement for life; in these days, decreasing of the fresh water increases the importance of the aquifer water. However, Upper Egypt is higher than north Egypt, so the water map continually changes daily, and the aquifer water is deeper than 10 m. The ground penetrating radar (GPR) system is used for underground water detection. GPR is a promising technology to detect and identify aquifer water or nonmetallic mines. One of the most serious components for the performance of GPR is the antenna system. The technology of the remote sensing and radar is rapidly developing, and it has led to the ultra-wideband electronic systems. All of these factors, such as miniaturized, low cost, possible compromise solution between depth and resolution, scanning in real time, easy to interpret, and decreased the false alarm, are important in designing the ground penetrating system. The electrical properties of the sand and fresh water layers are investigated using laboratory measurement and EM simulation. Different types of antenna may be used in GPR to operate over a frequency range for different penetration depth. Frequency-modulated continuous wave is also used for GPR and for through-the-wall applications. However, most of these kinds of antennas are limited by their large volume for certain applications. Therefore, a compact Vivaldi antenna with EBG and a compact planar printed quasi-Yagi antenna with mean-dered ground plane are designed to fulfill all above requirement.

**Keywords:** high-frequency structure simulator (HFSS), Yagi antenna, Vivaldi antenna, ultra-wideband (UWB), ground-penetrating radar (GPR), water detection, printed antenna, reflection coefficient, phase

## 1. Introduction

After the year 2002, ultra-wideband (UWB) systems have gained popularity mainly when the US Department of Federal Communications Commission (FCC) allocated a license-free spectrum for industrial and scientific purposes. FCC is doing the greatest step in opening new doors of researches for UWB in the field of wireless communications and microwave imaging [1, 2]. UWB device is defined as any device operating in absolute bandwidth greater than 500 MHz or fractional bandwidth greater than 0.2 of central frequency [3]. The frequency band ranges of UWB extended from 3.1 to 10.6 GHz that have expected the applications in the fields of wireless body area networks (WBAN), wireless local area networks (WLAN), wireless interoperability for microwave access (WiMAX), wireless personal area networks (WPAN), and ground-penetrating radar (GPR) technology where wide bandwidth is required [4]. GPR is the major applications of UWB technology, which

is in large degree used in military and civilian applications such as water detection and land mines [5]. There are many UWB antennas have been designed for GPR applications. The study based on the lower-frequency band is conducted mainly to increase the penetration depth, while the designing in the higher-frequency band is performed to achieve high-resolution imaging for GPR systems. Some of the researches focused on the entire UWB frequency range to further improve the bandwidth, while others focused on enhancement of the antenna gain [6]. Moreover, GPR is also used in remote-sensing techniques as nondestructive testing of concrete and detection of trapped people under debris or in opaque environment [7]. For the achievement of UWB GPR systems, the performance of various antenna designs, such as bow-tie antenna [8], spiral antenna [9], loaded dipole antenna [10], TEM horn antenna [11], tapered slot antenna (TSA) [12, 13], and Vivaldi antenna [14, 15], has been evaluated.

Ultra-wideband antenna is one of the preferred antennas for some applications in the microwave imaging, object measurement technology, and noninvasive testing (NIT) [4–15]. In this era, the microstrip antenna has the advantages of small size, high gain, and low cost for good performance in some applications [6–10]. Ground-penetrating radar (GPR) has been utilized by emitting an electromagnetic wave directed into the ground, and the buried objects cause reflections of the emitted wave that are then detected by the receiver system. This is contrasted in the electrical properties as the signal reflection coefficient and their related phase [11–17]. GPR has an ability to detect the electrical inhomogeneity of metal and dielectric object in the presence of surrounding soil or sand [18]. GPR system can exist at the same location for the transmitting and receiving, and there are four types of GPR system: quasi-monostatic radar if there is no separation distance between transmitter and receiver, monostatic radar if there is single antenna performs both transmit and receive operations [19], bistatic radar if the transmitter and receiver have separate distance, and multistatic radar if a radar system involves one or more transmitting platforms and multiple receiving platforms [20]. GPR systems have been classified as the time domain (impulse radars) and continuous wave (CW) radar [21]. CW radar transmits the signal, which can be frequency-modulated continuous wave (FMCW), or creates the resulting signal as a combination of monochromatic steps through a certain band of frequencies, referred as stepped frequency continuous wave (SFCW) [22]. GPR systems usually work at central frequencies below 1 GHz, and large bandwidth is needed for a better depth resolution and detailed echo. The use of impulse wideband systems involves some technical problems, such as Doppler processing, propagation fading, interference rejection, wave clutter, detecting birds on or near the water surface, and radar interference.

## **2. GPR system**

Egypt desert water, land mines, and Egyptian ancient mummy detection are an important, and yet challenging problem remains to be solved and is a matter of concern for both civilian groups and military. Water depth, quantity, and volume are different from location to another, and landmines have huge variety in use with various sizes and materials. They are mostly designed in a circular, rectangular, butterfly, or cylindrical shapes as V69, PSM-1, Hamdy, and Mon 200 with dimensions 13, 7.6, 21, and 43 cm, respectively. On the one hand, the electrical properties of water purity are changed due to water quantities and mineral contained; on the other hand, the electrical properties of the mummy are varying according to biological materials involved as tissues, bones, scapula, and femur, respectively [23]. The average effective dielectric constant is equal to 6.5 and dielectric loss equal to 15 [24].

Groundwater is a hidden natural resource. It is found in different proportions, in various rock types, and at various depths of ground surface. Previously, in the past, when there is no visible flow of water along the rivers or lakes, people used to dig small pits, in the river alluvium, then collect the groundwater coming through seepage to use in different purposes and for meeting the domestic needs. As well as the people of mountainous area, springs are the outcome of seepage from any groundwater system [25, 26].

More than 60% of the global population thrives by using only the groundwater resources. The groundwater, which was existing at shallow depths in the open wells, has gone deep due to overexploitation. Exploring these water sources becomes a challenging task to geoscientists [27–29].

As the signal of the GPR is required to propagate through inhomogeneous media, the efficiency of the antenna should be taken into account. Thus, in order to enhance the efficiency, a compact shape of Vivaldi is designed [7]. The compactness in the shape of antenna is achieved by using two Vivaldi surface shapes with the same feeding network. Frequency-modulated continuous wave (FMCW) is another type than pulse wave also used for GPR and for through-the-wall applications. FMCW systems are transmitting a repetitive waveform with increasing or decreasing frequency [21]. UWB-FMCW systems require a linear sweep, which may be difficult to create. Lower-frequency signals are required to penetrate the ground effectively as the penetration depth decreases with increasing frequencies.

GPR radar could be used for soil with different electrical properties to detect water underground [30, 31]. However, a broadband signal with good resolving power is required. Thus, the GPR antenna should operate on lower frequency and should have a very wide bandwidth. Also, the UWB antenna applied to communication system with high gain is highly desired [32].

### 3. Compact ultra-wideband (UWB) Vivaldi antenna

The main object of this section is the detection of water. A compact novel shape of Vivaldi antenna as shown in **Figure 1** with dimensions of  $0.17\lambda \times 0.16\lambda \times 0.013\lambda$  is proposed in this section [6].

A comparative study was undertaken as shown in **Table 1** for different Vivaldi antenna that are used of GPR application in the same interesting operating frequencies [8–11] to show that the proposed antenna gives compact size with higher gain from 250 MHz up to 10 GHz.

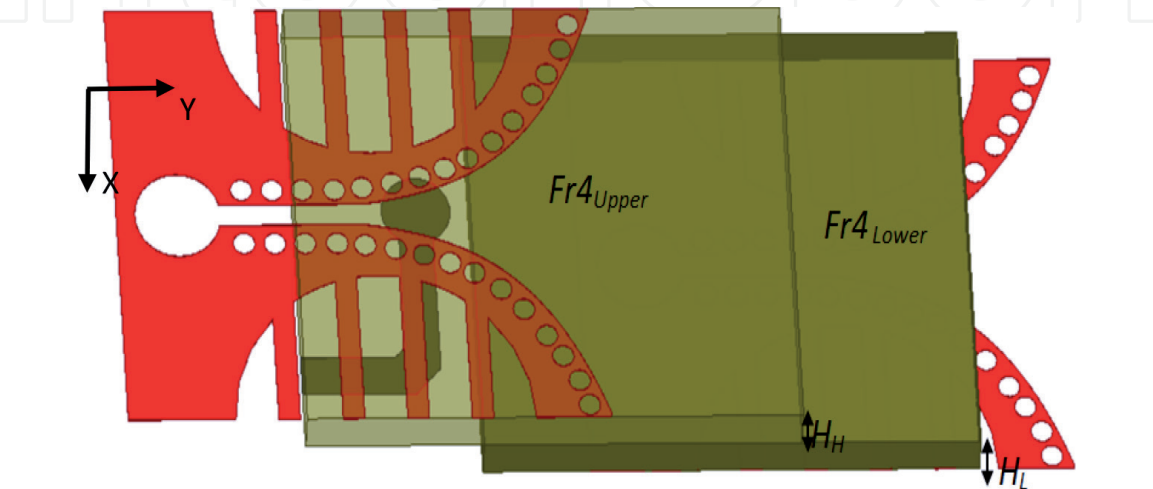


**Figure 1.**  
*3D geometry of the proposed Vivaldi antenna.*



Ref.	L × W cm <sup>2</sup>	Sub. thickness (cm)	Diel. properties	Gain (dBi)	BW (MHz)
[8]	60 × 40	0.32	ε <sub>r</sub> = 4.4, tan δ = 0.02	9	500–1500
[9]	60 × 30	0.315	ε <sub>r</sub> = 2.33, tan δ = 0.002	9	500–1500
[10]	7.8 × 7.5	0.16	ε <sub>r</sub> = 4.4, tan δ = 0.02	8	1000–4000
[11]	100 × 90	1	ε <sub>r</sub> = 4.4, tan δ = 0.02	10	50–250
Ours	13 × 12	2	ε <sub>r</sub> = 4.4, tan δ = 0.02	17	250–10,000

**Table 1.**  
*Comparison of the proposed antenna with other antennas (all dimensions in cm).*

There are a number of techniques used for improving the parameters of printed antennas with different feeding techniques. These techniques include electromagnetic bandgap (EBG), metamaterial, and defected ground structure (DGS). EBG structure has gained popularity among all the techniques reported for enhancing the parameters due to its simple structural design. The periodical shapes are etched as square, mushroom, and circular shapes in the radiator or ground plane to achieve inductive and capacitive load to create band-stop characteristics and to suppress higher mode harmonics and mutual coupling.

The basic concepts, working principles, and equivalent models of the different shapes of electromagnetic bandgap structure (EBG) are presented [36]. EBG has been used in the design of the Vivaldi antennas for improving the bandwidth and gain of proposed antenna and suppressing the higher harmonics mode and mutual coupling between adjacent elements. In addition, the proposed antenna cross-polarization is improved for the radiation characteristics [6].

3.1 Vivaldi antenna geometry and principle theory

A relatively large number of published UWB Vivaldi antennas consist of a feed line and exponential ground plane. Our proposed antenna starts as shown in **Figure 2(a)** from one layer of FR4 low-cost substrate with conventional exponential Vivaldi tapered slot line shape using empirical Eq.(1) [4]:

$$y = \pm 0.018 e^{0.27x} \tag{1}$$

where  $x$  and  $y$  are the axes of the inner and outer exponential to improve the impedance bandwidth. The first step is without any slot, **Figure 2(a)**, the second with circular EBG-etched slot on the edge of exponential tapered slot.

The symmetrical circular electromagnetic bandgap structure (EBG) slots are etched to increase the antenna bandwidth as shown in **Figure 2(b)**. The modified version from the first one is obtained by slotting the two arms of the Vivaldi antenna.

To improve the bandwidth of the Vivaldi antenna, symmetrical semicircular slots are etched to increase the antenna bandwidth as shown in **Figure 2(c)**.

**Figure 2(c)** and **(d)** shows the geometry of the proposed antenna in two different configurations. The substrate used is FR4 dielectric substrate of thickness 1 cm, a relative permittivity of 4.4 and a loss tangent of 0.02.

Finally, dual FR4 substrates printed with Vivaldi ground plane with the same feeding line are used. The final geometry of the proposed antenna design with ground plane and feeding network is shown in **Figure 3**. This design is used to investigate a dual substrate layer of Vivaldi ground plane antenna as shown in **Figure 3(a)** with the same feeding network as shown in **Figure 3(b)**. Proposed Vivaldi antenna consists of two layers from the dielectric sheet, the feeding line is sandwiched between them, and the two layers of metallic Vivaldi are mounted on

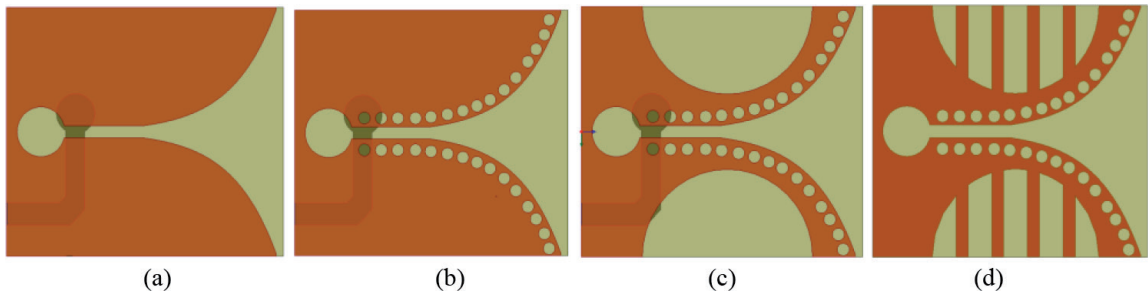


**Figure 2.**  
The top view of Vivaldi antenna, (a) conventional Vivaldi, (b–d) modified Vivaldi antenna.

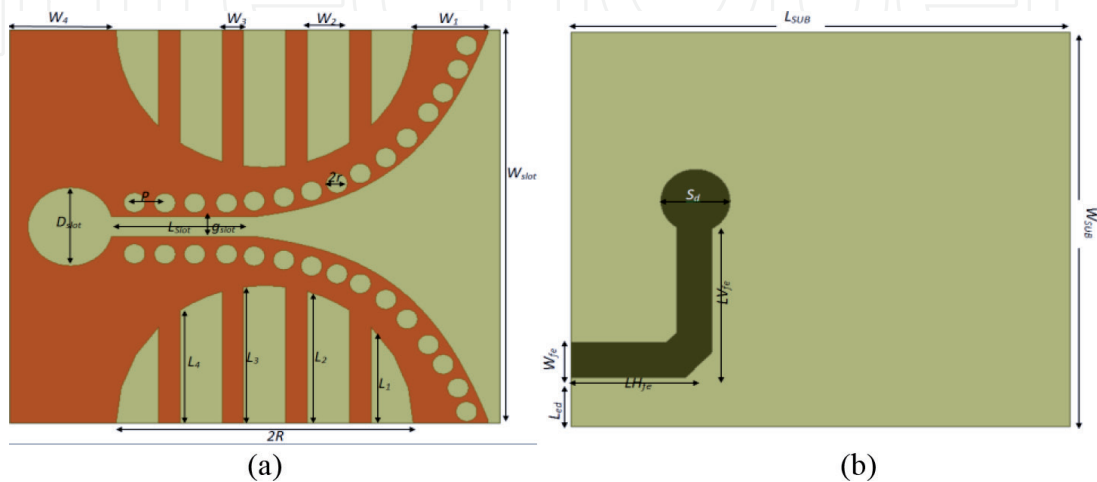


**Figure 3.**  
Geometry of the proposed Vivaldi antenna (a) ground plane and (b) feed line.

the dielectric substrate (one at the top and the other at the bottom) as shown in three dimensions of the proposed Vivaldi antenna in **Figures 1** and **7**.

### 3.2 Antenna simulation and measured results

The reflection coefficients of the antenna versus frequency for the four-step design of Vivaldi antennas in frequency range from 0.25 to 10 GHz are shown in **Figure 4(a)**, and the zooming range from 0.25 to 2 GHz is shown in **Figure 4(b)**. The final antenna design achieves improvement in antenna impedance matching all over the band. The dimensions of the proposed antennas are shown in **Table 2**.

The surface current density distributions of the compact Vivaldi antenna is shown in **Figure 5** at different resonant frequencies 0.4, 0.5, 0.75, 1.5, 1.75, and 2 GHz. The current distribution of the proposed antenna is studied to verify the operation of the proposed Vivaldi antenna. The exponential edge is responsible for the fundamental resonant frequency of the proposed antenna at 1.75 GHz as shown in **Figure 5**. The semicircular slots are etched to create the frequencies at 0.5 and 0.75 GHz. By adding stubs with different lengths, they are affecting the resonance from 1 to 2 GHz. The highest magnitude of current (red) is related to the corresponding radiating element. The simulated antenna gain of single and dual substrate is shown in **Figure 6(a)**. The gain gives better performance by using dual substrate layer, and it increases from 8 to 17 dBi in average over the operating band from 0.2 to 2 GHz. The average radiation efficiency is around 80% over the operating band for dual substrate, while its value is 50% for single substrate as shown in **Figure 6(b)**.

To validate the simulated results of the proposed antennas with single and dual substrate, they are fabricated by using printed circuit board (photolithographic)

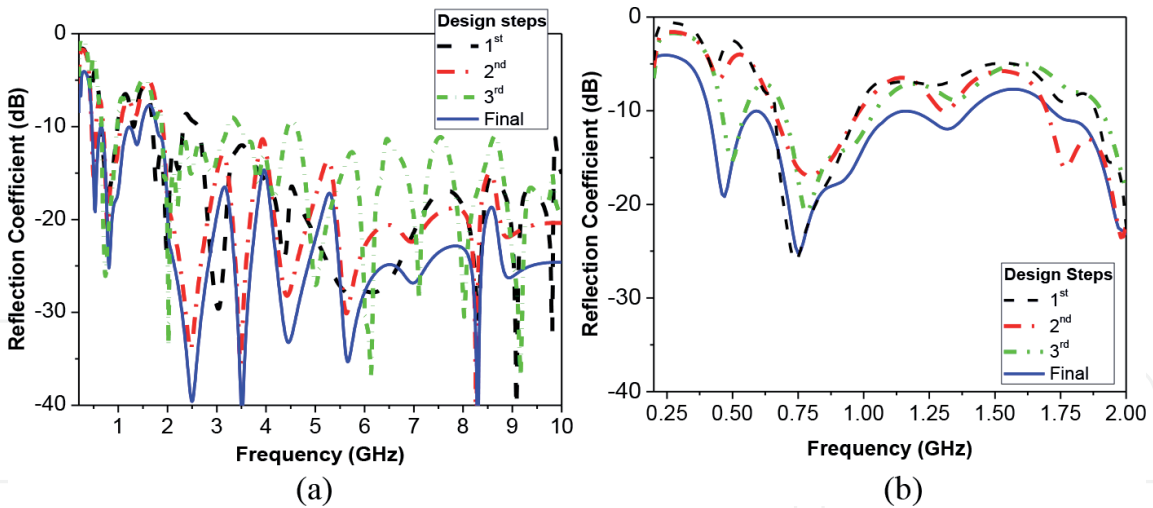


**Figure 4.**  $|S_{11}|$  versus frequency for the design steps of the proposed antennas (a) whole operating band and (b) zoom on low operating frequency.

<i>Lsub</i>	<i>Wsub</i>	<i>2R</i>	<i>Wslot</i>	<i>W1</i>	<i>W2</i>	<i>W3</i>	
13	12	8	11.5	2.1	1.2	0.6	
<i>W4</i>	<i>L1</i>	<i>L2</i>	<i>L3</i>	<i>L4</i>	<i>Dslot</i>	<i>Lslot</i>	<i>gslot</i>
3	3	4	4	3	2.4	4	0.6
<i>LVfe</i>	<i>LHfe</i>	<i>Wfe</i>	<i>Led</i>	<i>Sd</i>	<i>P</i>	<i>2r</i>	
4.5	3.5	1.1	1.5	1.9	0.9	0.6	

**Table 2.** Dimensions of the proposed antenna (all dimensions in cm).

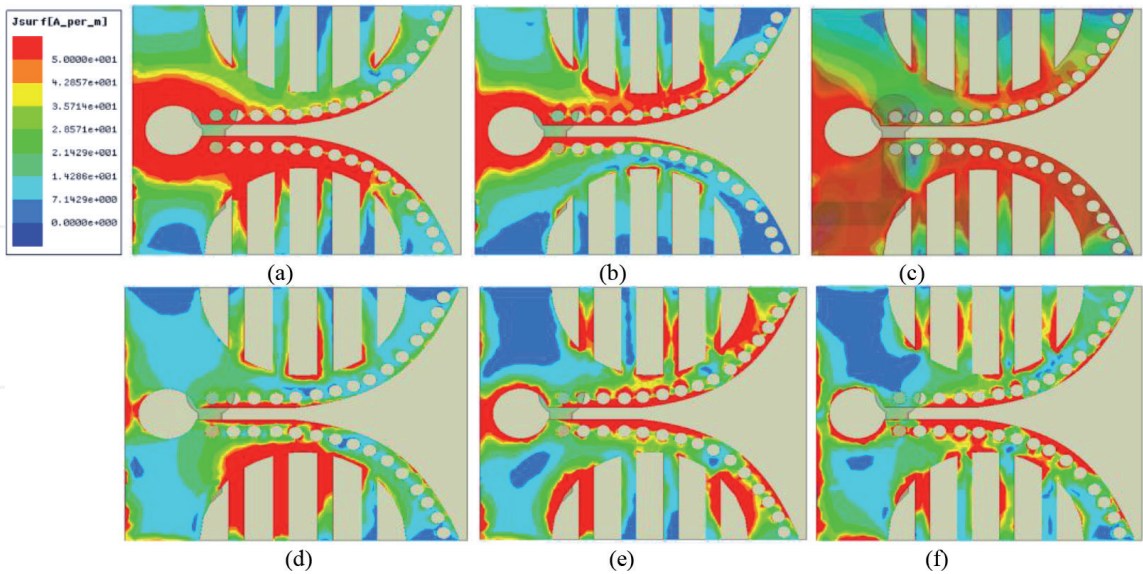


**Figure 5.** (a–f) Surface current densities for proposed Vivaldi antenna at 0.4, 0.5, 0.75, 1.5, 1.75, and 2 GHz, respectively.

technology and measured by using Agilent vector network analyzer technologies “Field Fox” Microwave Analyzer N9918A 26.5 GHz. **Figure 7** shows the photo of the fabricated antenna, feeding line, and Vivaldi antenna with dual substrate. The comparison between the measured and simulated results has been performed for the proposed Vivaldi antenna with single substrate that indicates good agreement.

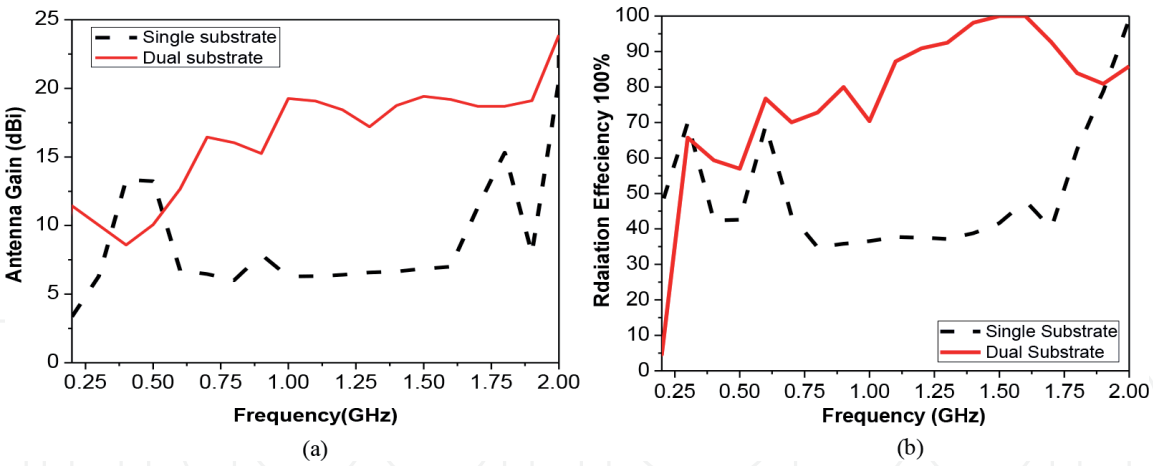


**Figure 6.**  
(a) Vivaldi antenna gain variation versus frequency and (b) radiation efficiency versus frequency of the proposed antenna.

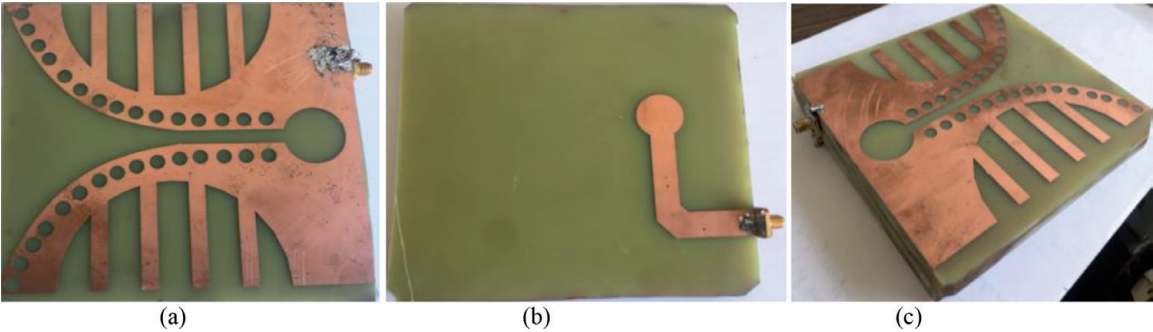


**Figure 7.**  
Photo of the fabricated antenna, (a) top view of one substrate, (b) the feeding line, and (c) 3D of dual substrate.

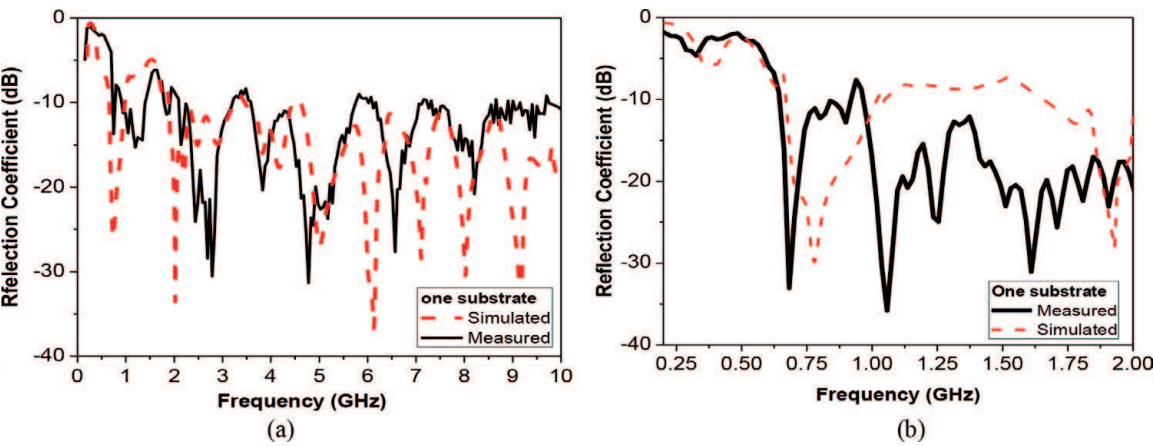


**Figure 8.**  
Reflection coefficient versus frequency for the proposed one substrate layer of Vivaldi antenna.

**Figure 8(a)** shows the whole range of the operation presenting proposed antenna from 0.2 to 10 GHz, while **Figure 8(b)** shows the zoom-operating range from 0.2 to 2 GHz. The measured reflection coefficient of proposed Vivaldi antenna with dual substrate is shown in **Figure 9**. **Figure 9(a)** shows the whole range from 0.2 to 10 GHz, while **Figure 9(b)** shows the zoom-operating range from 0.2 to 2 GHz. One can notice that there is a slight difference between the measured and simulated results of the reflection coefficient due to soldering of feeding launcher and fabrication tolerances.



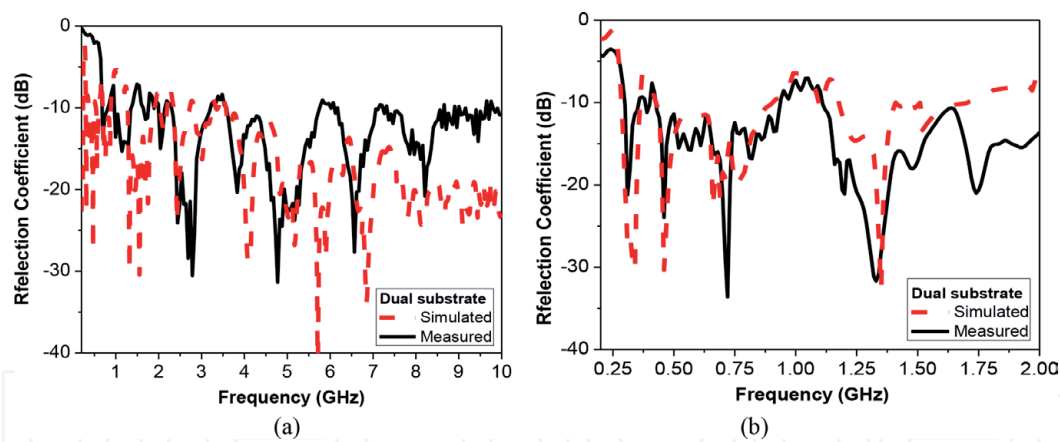


**Figure 9.**  
Reflection coefficient versus frequency for the proposed two substrate layers of Vivaldi antenna.

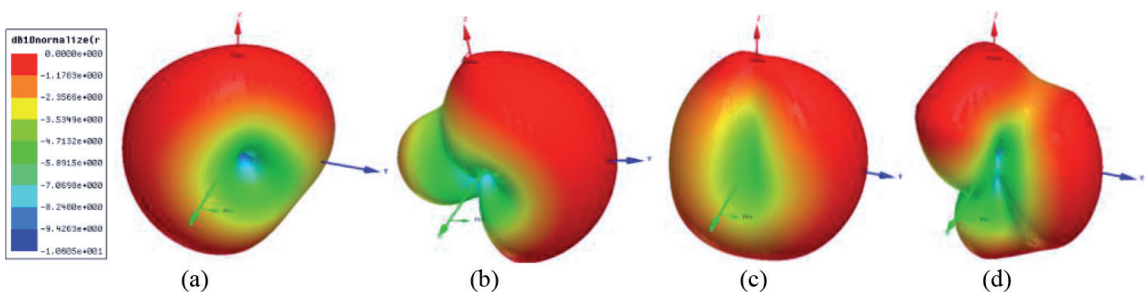


**Figure 10.**  
(a–d) 3D radiation pattern of dual layer substrate at 0.5, 1, 1.5, and 2 GHz, respectively.

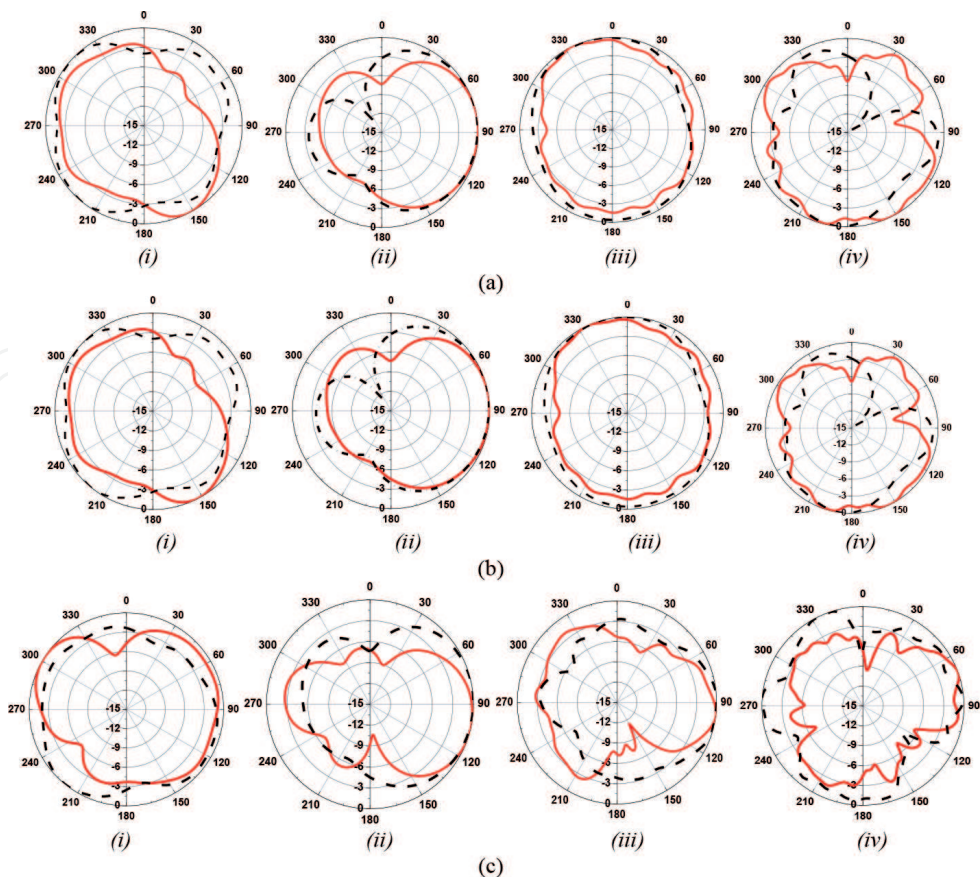


**Figure 11.**  
From (i) to (iv) 2D radiation pattern at 0.5 GHz, 1 GHz, 1.5 GHz, and 2 GHz, respectively, of single and dual substrate (a)  $\Phi^\circ=0^\circ$ , (b)  $\Phi^\circ=90^\circ$ , of single and dual substrate, and (c) from (i) to (iv)  $\theta=90^\circ$ , (--- one substrate antenna, and — dual substrate antenna).

**Figure 10** shows the three-dimensional radiation patterns of the proposed dual substrate Vivaldi antenna at different operating frequencies within the operating band at 0.5, 1, 1.5, and 2 GHz. The radiation patterns correspond to the axes shown in **Figure 1**. In the antenna, the radiator and the ground plane are participating to radiation. End-fire radiation pattern is an important requirement for ultra-wideband GPR application system. At lower frequencies of operation, the pattern resembles a conventional dipole antenna, but at higher end of the UWB spectrum, a few ripples are observed which is due to higher-order modes.

#### 4. Printed quasi-Yagi antenna with size reduction for water detection

Nowadays, quasi-Yagi printed antenna is extensively used in modern radar systems due to some advantages as high directivity, good radiation efficiency, affordable, low profile, and easy fabrication [33-35, 37]. However, the disadvantage of these antennas is narrow bandwidth, which achieves about 10%. So, the microstrip-fed quasi-Yagi antenna was initially introduced in 1991 [38] to improve the bandwidth of planar printed quasi-Yagi antennas, and many designs have been reported in [39]. A quasi-Yagi antenna based on microstrip-to-slot-line transition structure was presented in [40]. Modified wideband microstrip-to-coplanar strip-line (CPS) balun was used in quasi-Yagi antenna designs for increasing the antenna bandwidth [41]. Approximately 48 and 38.3% bandwidths were achieved by using the microstrip-to-coplanar strip-line transition structures in [42] and [43], respectively. However, the antenna bandwidths are still restricted by the delay line used in the balun structures. Coplanar waveguide feeding or ultra-wideband balun was presented to improve the bandwidth in some designs [44]. A broad bandwidth of 44% was obtained in [45]. However, the asymmetric nature of the printed quasi-Yagi antenna deteriorates the unidirectional radiation patterns. An ultra-wide band balun feeding structure in which the balun was realized via holes was used in quasi-Yagi antenna for wideband in [46]. Slot and CPS-fed feeding structures were also used in planar printed quasi-Yagi antenna to increase the bandwidth. The maximum available bandwidth of these techniques is about 55%. To improve the bandwidth of quasi-Yagi antenna by modifying the driver to a tapered driver or bowtie driver, rapid developing technology of remote sensing and radar has led to the ultra-wide band (UWB) electronic systems.

##### 4.1 Antenna design and geometry

**Figure 12** shows the geometric structure and parameters of the proposed planar quasi-Yagi antenna. This antenna is printed on commercial thick FR4 substrate and a thickness of 9.5 mm. The antenna consists of a microstrip-line-to-slot-line transition structure, a meandered driver T-shaped dipole and two meandered parasitic strips on top layer. The feeding system is printed on the other substrate side with lengths  $L_f$  and  $S_D$  with a circular resonator. The circular resonator is used to match the input impedance of the antenna to a 50  $\Omega$  feeding line. The dimension of the substrate width and length are  $72 \times 70 \text{ cm}^2$ . For matching the antenna, a  $\lambda/4$  slot line ended with a circular slot of diameter  $L_D$  is used.

The traditional printed quasi-Yagi antenna started to resonate from 90 MHz as shown in **Figure 13(a)**. Folded stub ground plane and driven dipole that is etched in order to reduce the size of the printed quasi-Yagi antenna, as shown in **Figure 13(b)**, are employed. The ground plane width and the driver dipole length are equal. The antenna shown in **Figure 13(b)** has 80 MHz as the lowest frequency. Since the ground plane has reduced size, the bandwidth of the antenna is reduced. A driver meander

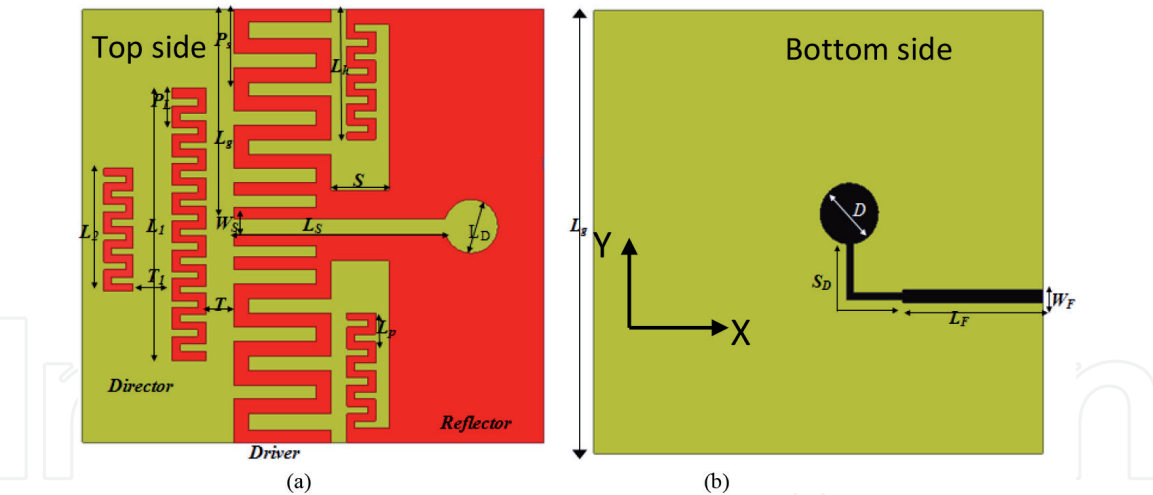


**Figure 12.**  
The quasi-Yagi antenna configuration (a) upper and (b) bottom layer [37].

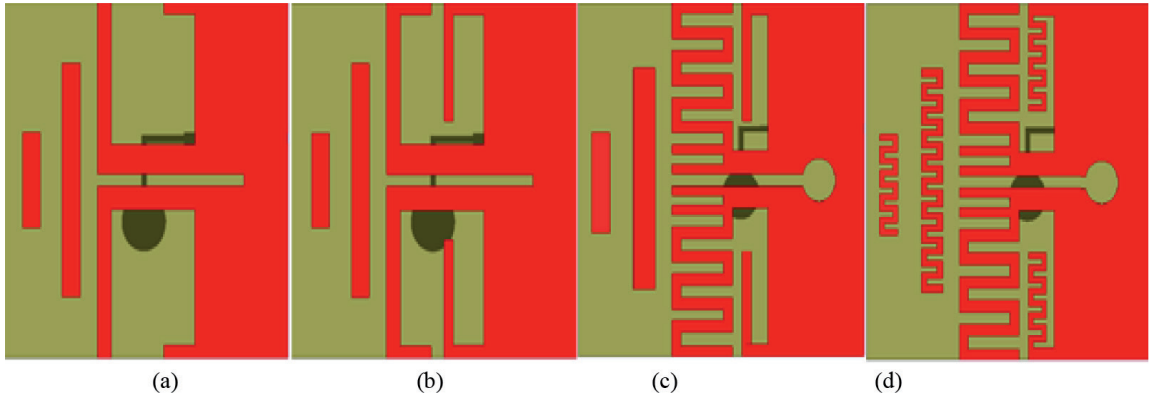


**Figure 13.**  
The compact printed quasi-Yagi antenna design steps [37].

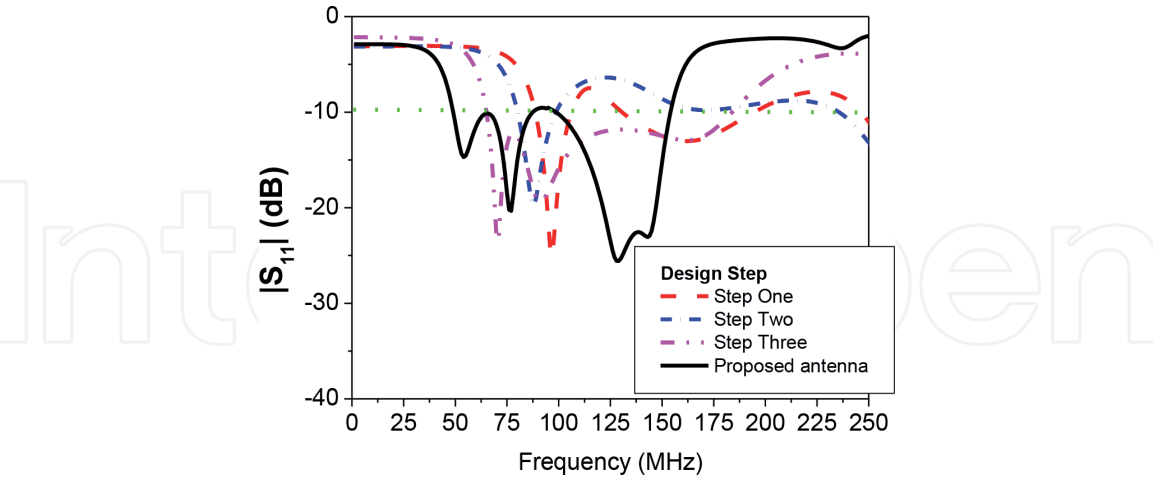


**Figure 14.**  
Simulated  $|S_{11}|$  of the design steps as shown in Figure 11 [37].

dipole is etched to increase the electrical size of the antenna (**Figure 13(c)**). The antenna started to operate from 62.5 to 185 MHz. Two meandered stubs are symmetrically extended from its ground plane as shown in **Figure 13(d)**. The reflection coefficients  $|S_{11}|$  of the antenna design procedure are shown in **Figure 14**.

As shown, the antenna consists of a circular balun feeding which takes the form of a curved microstrip line step transition, in addition to a printed dipole, a ground plane, and two parasitic strips. The larger dipole is located at a distance  $S$  away from the ground plane which has a greater length than the larger dipole itself, so it can act



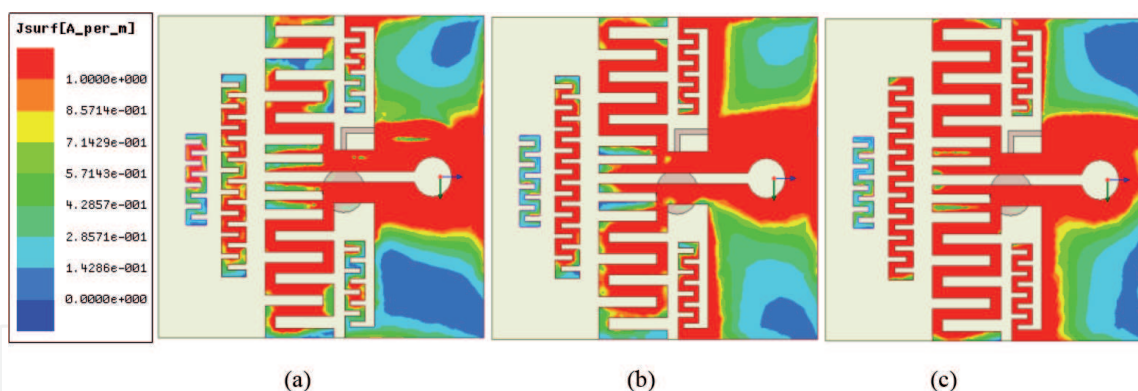


**Figure 15.**  
The surface current distribution of the printed quasi-Yagi antenna at (a) 50, (b) 100, and 150 MHz [37].

as a reflector. On the second size of the substrate, the two dipoles are located, their line length is 2.6 cm, and the two parasitic spacing was optimized using the reading-made software package HFSS ver.14 in order to improve the antenna performance which means that it has a wide bandwidth, stable radiation, moderate gain, and high front-to-back ratio.

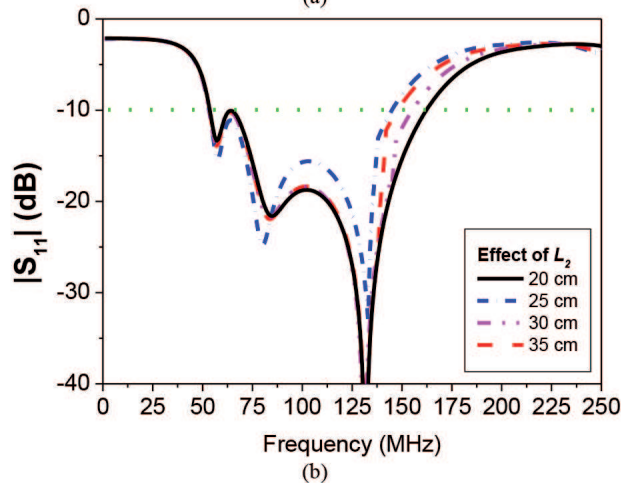
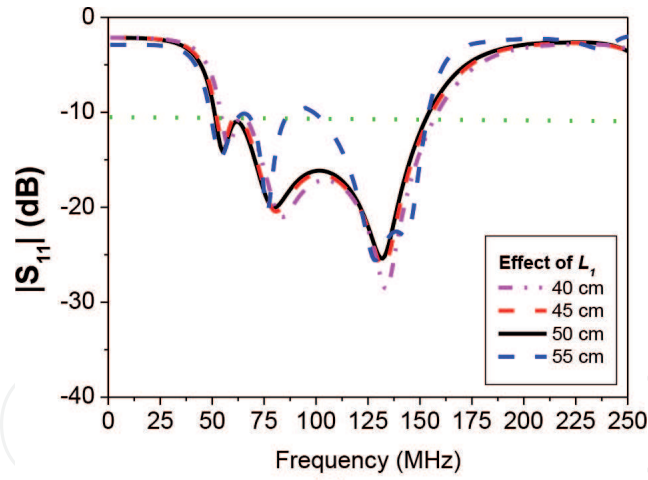
In quasi-Yagi antenna design, metallic strip is always used as a director. To improve the directivity and impedance matching in the high-frequency band, the two metallic strips are used. The simulated surface current distributions of the proposed antenna at 50, 100, and 150 MHz are shown in **Figure 15**. The directors have weak surface current as shown in **Figure 15**, while the two parasitic strips have a large magnitude of surface current at 50 MHz. the largest value of surface current at resonant 100 MHz takes place at larger parasitic strip and the driven dipole. At 150 MHz, the current concentrates on the meandered driven dipole. Compared to **Figure 15**, the surface currents on the metallic strips are enhanced, which means that the effects of the parasitic strips as directors improved the antenna performance at the high-frequency band.

## 4.2 Antenna parameter study

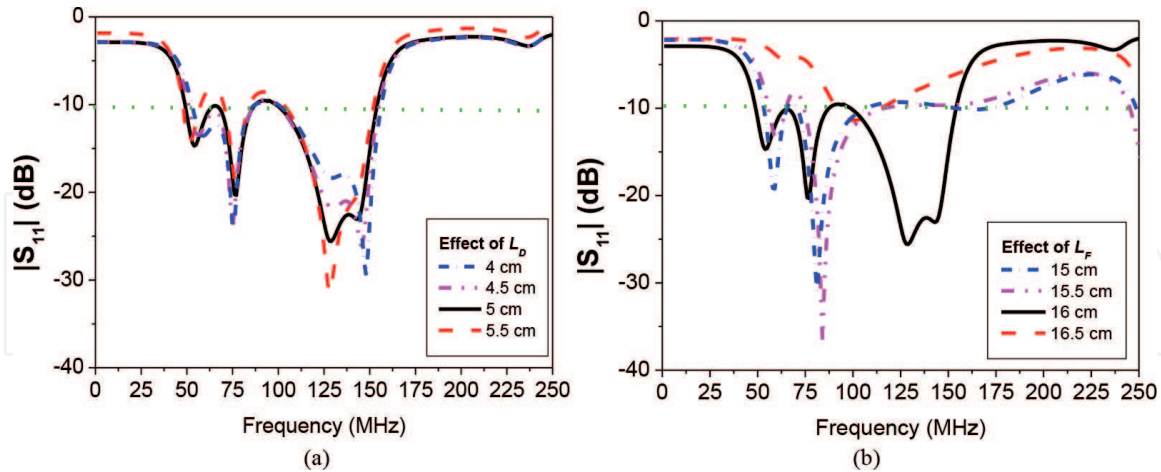
The antenna structure was optimized to operate at 100 MHz center frequency. The reflection coefficient against frequency for different values of  $L_1$  is shown in **Figure 16(a)**. As the value of  $L_1$  is increased (in steps from 40 to 55 cm), the resonance frequency decreased. At  $L_1 = 50$  cm, the antenna provides the largest beamwidth. One can say that the resonant frequency of the lower band is mainly determined by the length of the larger strip. The dipole in this antenna acts as director of quasi-Yagi antenna. Also, simulation was done to see the effect of  $L_2$  on the antenna bandwidth. **Figure 16(b)** shows  $S_{11}$  against frequency for different values of  $L_2$ , which shows that as  $L_2$  increased from 20 to 35 cm, the highest frequency almost did not change, while the lower resonance (50 MHz) slightly changed. When the ground plane circular slot  $L_D$  was changed from 4 to 5.5 cm, impedance matching was affected, while the lower and higher frequency did not change (**Figure 17(a)**). One can conclude that the diameter of the slot affects the feeding impedance. The effect of the feeding length  $L_f$  was studied as shown in **Figure 17(b)**.  $L_f$  was varied from 15 to 16.5 cm which caused noticeable changes in the operating frequency band and the value of the reflection coefficient. The length  $L_f$  highly affects the impedance matching, and the optimized length of the feeding is 16 cm. **Figure 18(a)** shows the reflection coefficient of the antenna as a function of the spacing between the driver and director ( $T$  and  $T_1$ ).

Increments of the spacing decreased the coupling effect between the parasitic element and the dipole induced significant changes in the reflection coefficient in the operating band region from 50 to 150 MHz, but negligible changes occur in the bandwidth.



**Figure 16.**

Effect of the length (a)  $L_1$  and (b)  $L_2$  on the simulated reflection coefficient [37].

**Figure 17.**

Effect of the length (a)  $L_D$  and (b)  $L_F$  on the simulated reflection coefficient [37].

In the high-frequency region of 100 MHz band, the antenna performance is affected mainly by the spacing between the driver and the director. The quasi-Yagi antenna and the T-dipole were designed to operate at 50 and 150 MHz, which shows that a suitable choice of this spacing is very important for the wideband operation of the proposed antenna.

The reflection coefficient  $S_{11}$  against frequency is shown in **Figure 19** for different values of the parameter  $D$  (balun circle) and  $S_D$  (length from the feeding). The lower resonance and impedance matching are varied as  $D$  increases from 4 to

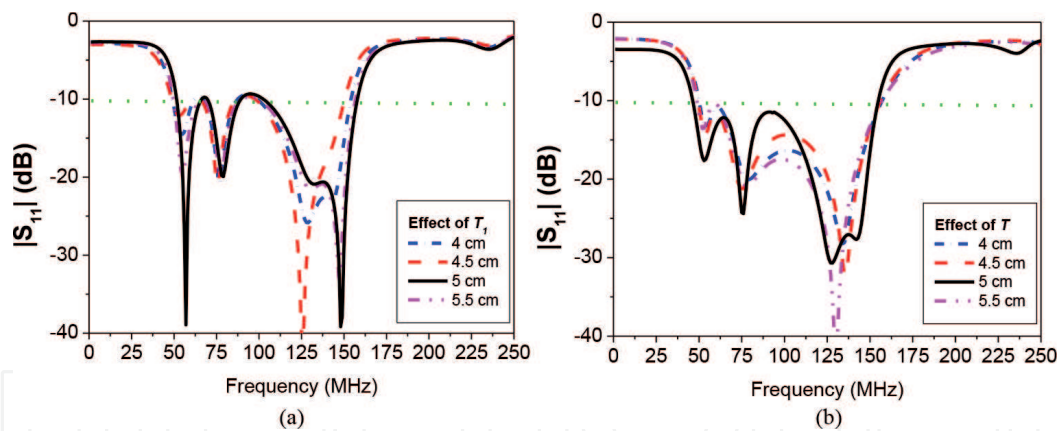


**Figure 18.**  
Effect of the length (a)  $T_1$  and (b)  $T$  on the simulated reflection coefficient.

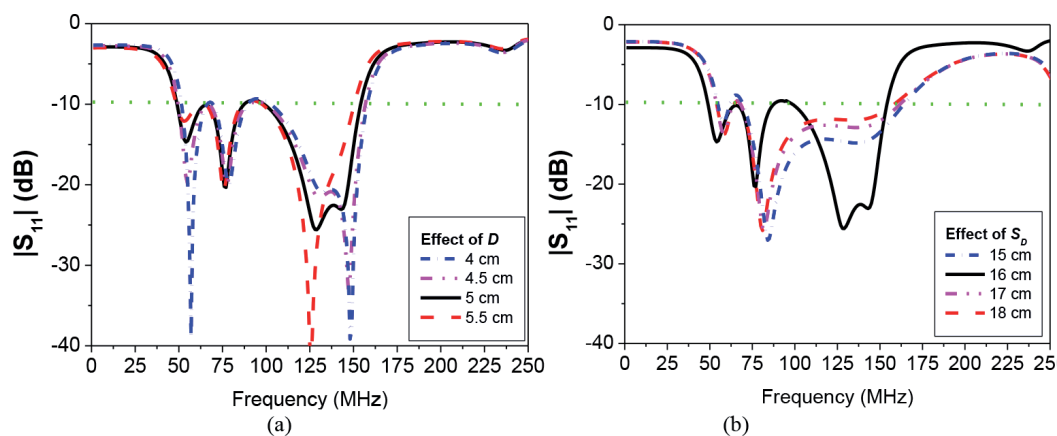


**Figure 19.**  
Effect of the length (a)  $D$  and (b)  $S_D$  on the simulated reflection coefficient.

5.5 cm. As the value of  $S_D$  is changed from 15 to 18 cm, the behavior of  $S_{11}$  is changed significantly, so the choice of  $S_D$  is very important for the operation of the antenna.

### 4.3 Ground-penetrating radar antenna system

FMCW GPR system is used for the detection of underground water in the frequency range from 50 to 150 MHz. **Figure 20(a)** shows the radar system which requires a high-gain antenna to obtain acceptable scanning resolution. We used laboratory measurement and EM simulation in order to investigate the electrical and physical properties of the sand and fresh water. The simulated parameters depend on the Debye dispersive model inherent in HFSS software package. **Figure 20(b)** shows the study of the ground effect on the radiation characteristics of the antenna  $S_{11}$  projection. The distance  $K$  between the antenna and the ground surface was increased from up to 100 cm. The volume of the sand layer was  $300 \times 200 \times 200 \text{ cm}^3$ . **Figure 21** shows the reflection with and without the sand layer. It was found that in order to keep  $S_{11}$  very close from the case of free space,  $K$  should not be less than 50 cm. **Figure 22** shows both the gain and radiation efficiency. It is clear that the gain was increased by about 1.5 dBi compared to the case of free space, which may be attributed to the increase in directivity at certain frequencies, while it remains unchanged in other frequencies. The antenna radiation efficiency, as indicated from **Figure 22**, is reduced. The three-dimension radiation pattern of the proposed antenna in both cases is also studied at three different resonant frequencies 50, 100, and 150 MHz, respectively, as shown in **Table 3**, while the 2D radiation patterns at xy-plane ( $E\Phi$ ,  $E\theta$ ) at  $\Phi = 0^\circ$  and yz-plane

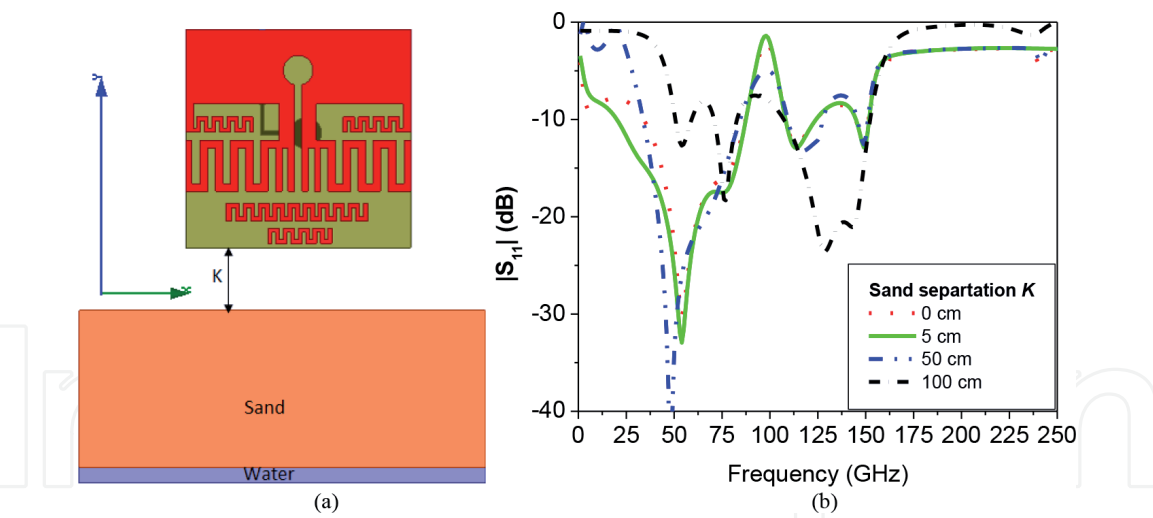


**Figure 20.**  
(a) The GPR antenna system for water detection and (b) the effect of  $K$  on proposed antenna reflection coefficient [37].

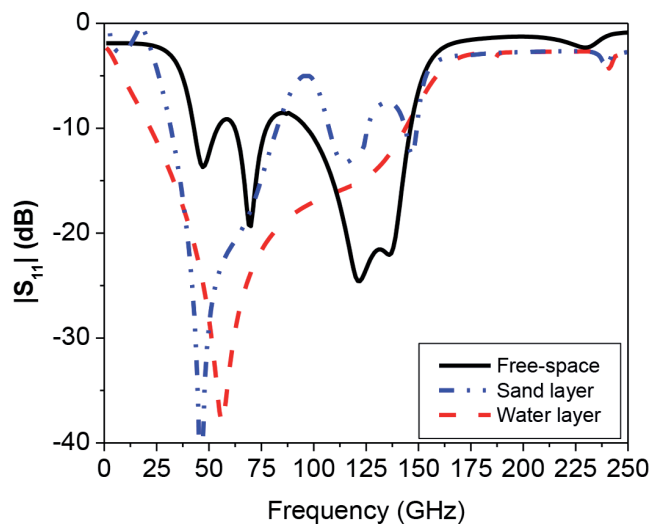


**Figure 21.**  
 $|S_{11}|$  of the receiver antenna in different cases at  $K = 50$  cm.

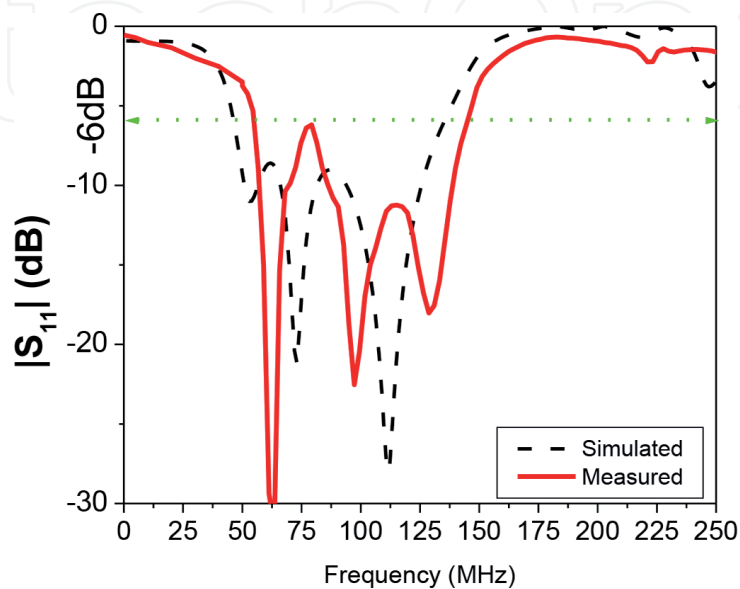


**Figure 22.**  
 $|S_{11}|$  comparison between measured and simulated reflection coefficient of the proposed antenna [37].

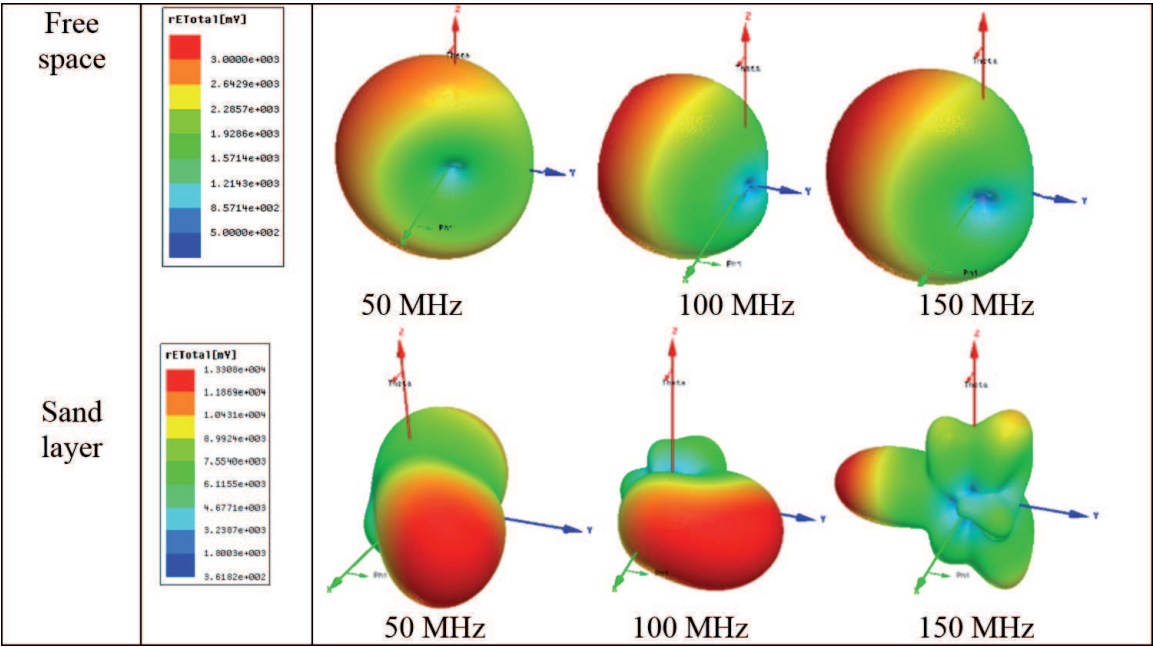


Table 3.  
The 3D radiation pattern at different resonant frequencies with and without sand layer

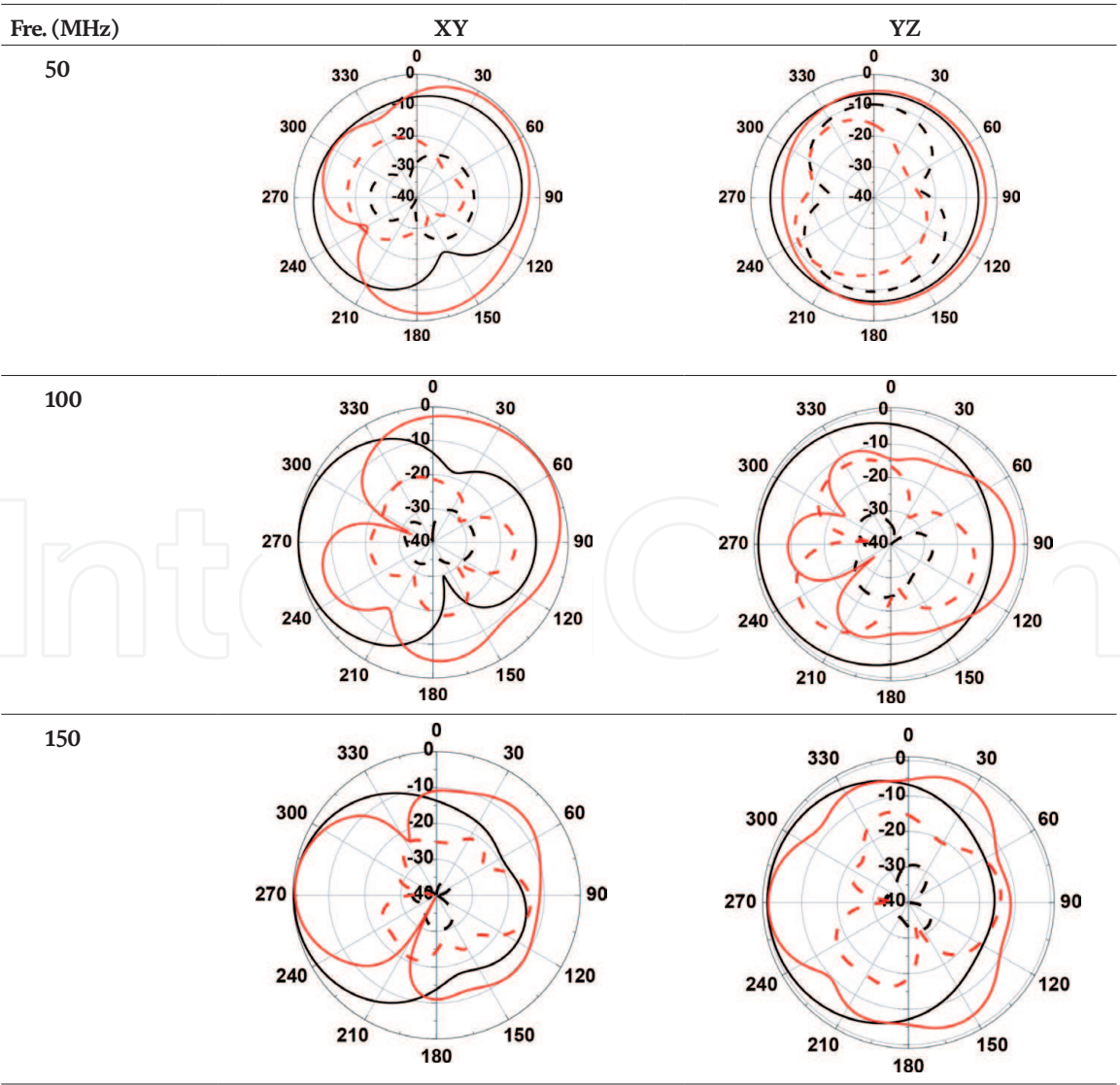
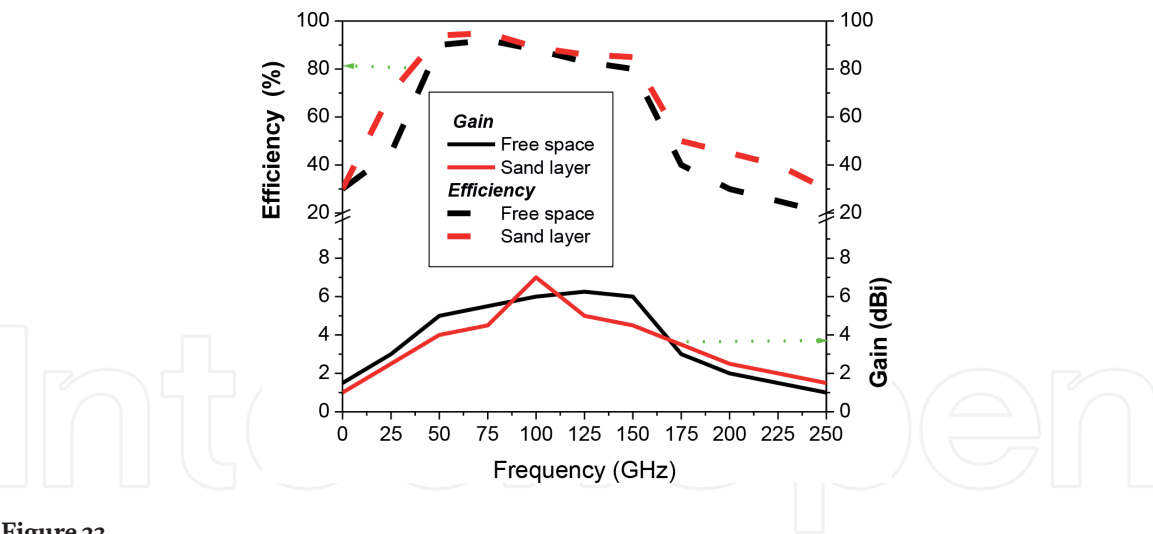


Table 4.  
The 2D  $E\Phi$  and  $E\theta$  ( $\phi = 90^\circ$  and  $\theta = 90^\circ$ ) at frequencies 50, 100, and 150 MHz with and without sand layer; black; without sand, red; with sand layer, solid line ( $E\Phi$ ) and dash line ( $E\theta$ ), respectively





**Figure 23.**  
The antenna gain and efficiency with and without sand layer [37].

( $E\Phi$ ,  $E\theta$ ) at  $\theta = 90^\circ$  of the original design are plotted in **Table 4** at the same frequencies. The two-dimensional radiation patterns at 50, 100, and 150 MHz with and without sand are plotted in **Table 4**. A slight change took place in the E-plane and H-plane radiation patterns keeping good directivity within the whole frequency band. The back lobes are below  $-5$  dB. Deterioration takes place in the H-plane (YZ plane) as the frequency increases especially in the high-frequency bands (e.g., 500 MHz).

#### 4.4 Fabrication and measurements

A photolithographic technique on FR4 substrate with  $100\ \mu\text{m}$  copper thickness was used to realize the proposed antenna. A  $50\ \Omega$  SMA launcher was used as a transition between the microstrip antenna and the coaxial line, which was not included in the simulation process. Rohde and Schwarz ZVA67 VNA was used to measure  $S_{11}$ . The antenna gain and radiation efficiency are also tested as shown in **Figure 23** in both cases namely free space and in the presence of sand layer. The antenna gain is also tested as shown in **Figure 23** in both cases namely free space and in the presence of sand layer. The proposed antenna performance is investigated with and without sand layer as shown in **Figure 20(a)**. The sufficient distance that keeps the antenna reflection coefficient near from free space is almost about 50 cm as shown in **Figure 20(b)**. **Figure 23** shows that the antenna radiation efficiency is increased at present of sand layer by 5%. While the antenna gain is reduced by about 1.5 dBi in the present of sand layer. The gain in the present of sand layer increases at certain resonant frequency due to increase in directivity and has value less than free space on the other resonant frequencies. The optimized antenna reflection coefficient is measured, and there is a good agreement with the simulated results. The measured bandwidth extends from 56 to 150 MHz for the  $-6$  dB reflection coefficient, while the simulated bandwidth extends from 45 to 140 MHz. This bandwidth completely covers the specification for operation.

The slight difference between the measured and simulated reflection coefficient could be from misalignment between curved microstrip line and the circular slot of the balun and effect of the SMA connector, in addition to some fabrication tolerances.

## 5. Conclusion

The importance of aquifer water increased these days after decreasing the fresh water. A precise approach for the detection of buried nonmetallic objects is ground-penetrating radar (GPR). It should be importance of aquifer water increased these days after decreasing the freshwater. A precise approach for the detection of buried nonmetallic objects is ground penetrating radar (GPR). A novel, miniaturized, and low-cost antennas, which compromise between depth and resolution for different applications, are highly needed. This requires hundreds of conducting research activities in this area. However, although GPR has shown some promising results, the complexity of the problem requires certain challenges on the operation of GPR systems. One of the most serious hardware components for the performance of ground-penetrating radar (GPR) is the antenna system. First, a new compact Vivaldi antenna is designed to achieve ultra-wideband extending from 0.4 to 10 GHz and high average gain of about 17 dBi with average radiation efficiency of about 80%. The proposed antenna consists of dual exponential Vivaldi shapes on both dielectric substrates with the same feeding network. The GPR results in frequency range extending from 0.4 to 2 GHz of the water detection have also been investigated under certain system parameters. Second, ultra-wideband printed quasi-Yagi antenna has been introduced. The proposed antenna has the advantage of simple single feed structure which consists of a circulator balun with a microstrip line and a circulator slot. The antenna bandwidth extends from 47 to 150 MHz based on  $-6$  dB reflection coefficient. The gains at the upper and lower bands are 3.5 and 6.5 dBi. It should be noted that the proposed antenna has the advantage of simple structure and stable end-fire radiation pattern, which makes it widely used in ground-penetrating radar. The average simulated gain in this band is about 5 dBi. At the same time, this antenna possesses low profile and miniaturization characteristics. Furthermore, the wide beamwidth and high gain can promise the antenna to be widely applied in many communication systems.

### Author details


Dalia N. Elsheakh<sup>1,2\*</sup> and Esmat A. Abdallah<sup>2</sup>

1 Hawaii Center for Advanced Communication (HCAC), Hawaii University, Honolulu, Hawaii, USA

2 Department of Microstrip, Electronics Research Institute, Giza, Egypt

\*Address all correspondence to: [dalia8@hawii.edu](mailto:dalia8@hawii.edu)

### IntechOpen

© 2019 The Author(s). Licensee IntechOpen. This chapter is distributed under the terms of the Creative Commons Attribution License (<http://creativecommons.org/licenses/by/3.0>), which permits unrestricted use, distribution, and reproduction in any medium, provided the original work is properly cited. 

## References

- [1] Federal Communications Committee. First Report and Order, Revision of Part 15 Commission's Rule Regarding Ultra Wideband Transmission Systems. FCC 02-48; 2002
- [2] Dastranj A. Wideband antipodal Vivaldi antenna with enhanced radiation pattern. *IET Microwaves, Antennas and Propagation*. 2015;**9**(15):1755-1760
- [3] Zheng Y, Guo C, Lin X, Yang X. Vivaldi antenna design in millimeter wave band with ultra wide bandwidth and high gain. In: *IEEE MTT-S Workshop Series on Advanced Materials and Processes of RF and THz Applications*, Chengdu, China. 2016. pp. 1-3
- [4] Pandey GK, Verma H, Meshram MK. Compact antipodal Vivaldi antenna for UWB applications. *Electronics Letters*. 2015;**51**(4):308-310
- [5] Elsheakh DN, Elsadek H, Abdallah EA. Microwave test. In: *Noninvasive Electromagnetic Biological Microwave Testing*. Rijeka . ISBN:978-953-51-2867-0: InTech; 2017
- [6] Elsheakh DN, Eltresy NA, Abdallah EA. Ultra wide bandwidth high gain Vivaldi antenna for wireless communications. In: *Progress in Electromagnetics Research Letter (PIERL)*. Vol. 69. 2017. pp. 105-111
- [7] Kalbhor G, Vyas M, Patil BP. Antenna design for ground penetrating radar system. *International Journal of Advanced Electrical and Electronics Engineering (IJAEEE)*. 2013;**2**(6):15
- [8] Karamzadeh S, Kiliç OF, Hepbiçer AS, Demirbaş F. Bow tie antenna design for GPR applications. *International Journal of Electronics, Mechanical and mechatronics Engineering*. 2016;**6**(2):1187-1194
- [9] Thaysen J, Jakobsen KB, Lenler-Eriksen H-R. Wideband cavity backed spiral antenna for stepped frequency ground penetrating radar. In: *IEEE Antennas and Propagation Society International Symposium*, Washington, DC, USA. 2005
- [10] Morrow IL, Persijn J, van Genderen P. Rolled edge ultra-wideband dipole antenna for GPR application. *IEEE AP-S International Symposium (Digest)*. 2002;**3**:484-487
- [11] Malherbe J, Barnes N. Tem horn antenna with an elliptic profile. *Microwave and Optical Technology Letters*. July 2007;**49**:1548-1551
- [12] Shao J, Fang G, Ji Y, Tan K, Yin H. A novel compact tapered-slot antenna for GPR applications. *IEEE Antennas and Wireless Propagation Letters*. 2013;**12**:972-975
- [13] Zhang F, Fang G-Y, Ji Y-C, Ju H-J, Shao J-J. A novel compact double exponentially tapered slot antenna (DETSA) for GPR applications. *IEEE Antennas and Wireless Propagation Letters*. 2011;**10**:195-198
- [14] Elsheakh DN, Abdallah EA. Compact shape of Vivaldi antenna for water detection by using ground penetrating radar (GPR). *Microwave and Optical Technology Letters*. 2014;**56**(8)
- [15] Elsheakh DM, Abdallah EA. Novel shapes of Vivaldi antenna for ground penetrating radar (GPR). In: *7th European Conference on Antenna and Propagation (EuCAP)*, Gothenburg. 2013. pp. 2886-2889
- [16] Atteia GE, Shaalan AA, Hussein KFA. Wideband partially-covered bowtie antenna for ground-penetrating radars. *Progress in Electromagnetics Research*. 2007;**71**:211-226

- [17] Diamanti N, Redman D, Giannopoulos A. A study of GPR vertical crack responses in pavement using field data and numerical modelling. In: 13th Int. Conf. Ground Penetrating Radar (GPR). Lecce, Italy; 2010
- [18] Jol HM. Ground Penetrating Radar Theory and Applications. 1st ed. Amsterdam: Elsevier Science; 2009
- [19] Carlotto MJ. Detecting buried mines in ground penetrating radar using a Hough transform approach. In: Battlespace Digitization and Network-Centric Warfare II. Orlando; 2002. pp. 251-261
- [20] Daniels DJ. Ground Penetrating Radar. 2nd ed. IET Radar, Sonar, Navigation and Avionics Series 152007
- [21] Hoole JG. Implementation of a Low-Cost FM-CW Radar. M.S. in Electronic Engineering at the University of Stellenbosch South Africa; 2008
- [22] Amiri A. Multi-band and dual polarized ultra-wide band horn antenna for landmine detection using ground penetrating radar technique. [Thesis submitted for the degree of Doctor of Philosophy]. University College London; 2015
- [23] Liu Y, Wang M, Cai Q. The target detection for GPR images based on curve fitting. In: 3rd International Congress on Image and Signal Processing. Yantai, China; 2010. pp. 2876-2879
- [24] Marshall Legacy Institute. Dogs for the Detection of Landmines. United states Institute of Peace; 2005
- [25] Bonham-Carter GF. Geographic Information Systems for Geoscientists: Modeling with GIS. New York: Pergamon Press; 1994
- [26] Bressan MA, Anjos CD. Techniques of remote sensing applied to the environmental analysis of part of an aquifer located in the São José Dos Campos region SP, Brazil Environmental Monitoring and Assessment. 2003;84:99-109
- [27] Bressan MA, Anjos CD. Techniques of remote sensing applied to the environmental analysis of part of an aquifer located in the São José Dos Campos region SP, Brazil. Environmental Monitoring and Assessment. 2003;84:99-109
- [28] Carranza EJM. "Geochemical Anomaly and Mineral Prospectivity Mapping in GIS" Handbook of Exploration and Environmental Geochemistry. Amsterdam: Elsevier; 2008
- [29] Carrière SD, Chalikakis K, Sénéchal G, Danquigny C, Emblanch C. Combining electrical resistivity tomography and ground penetrating radar to study geological structuring of karst unsaturated zone. Journal of Applied Geophysics. 2013;94:31-41
- [30] Pettinelli E, Burghignoli P, Pisani A, Ticconi F, Galli A, Vannaroni G, et al. Electromagnetic propagation of GPR signals in Martian subsurface scenarios including material losses and scattering. IEEE Transactions on Geoscience and Remote Sensing. 2007;45:1271-1281
- [31] Shaik AG, Siddiqui MAA. Dielectric properties of calcified tissue-the bone. International Journal of Science, Environment and Technology. 2013;2(6):1412-1420
- [32] Liang X. Analysis and research on several wide band antenna and fractal antenna. Dissertation for the doctor degree of Xi'an Jiaotong University, China; 1997
- [33] Rahim MKA, Karim MNA, Masri T, Asrokin A. Comparison between straight and U shape of ultrawide band microstrip antenna using log periodic technique. In: IEEE International



Conference on Ultra-Wideband, 2007. Vol. 2. ICUWB; 2007. pp. 696-699

[34] Kalbhor G, Vyas M, Patil BP. Antenna design for ground penetrating radar system. *International Journal of Advanced Electrical and Electronics Engineering (IJAEED)*. 2013;2(6):1-5

[35] DeJean GR, Thai TT, Nikolaou S, Tentzeris MM. Design and analysis of microstrip Bi-Yagi and quad-Yagi antenna arrays for WLAN applications. *IEEE Antennas and Wireless Propagation Letters*. 2007;6:244-248

[36] Elsheakh D. Electromagnetic band gap (EBG) structure for microstrip antenna systems (analysis and design)" [Thesis Submitted for the Degree of Doctor of Philosophy]. Ain Shams University faculty of Engineering, Electrical and Communication Dept.; 2015

[37] Elsheakh DN, Abdallah EA. Ultra wide band planar printed quasi-Yagi antenna with size reduction for water detection in the Egyptian Desert. *Microwave and Optical Technology Letters*. 2015;57(1):226-233

[38] Huang J, Demission AC. Microstrip Yagi array antenna for mobile satellite vehicle application. *IEEE Transactions on Antennas and Propagation*. 1991;39(7):1024-1030

[39] Han K, Park Y, Choo H, Park I. Broadband CPS-fed Yagi-Uda antenna. *Electronics Letters*. 2009;45(24):1207-1209

[40] Kan HK, Waterhouse RB, Abbosh AM, Bialkowski ME. Simple broadband planar CPW-fed quasi-Yagi antenna. *IEEE Antennas and Wireless Propagation Letters*. 2007;6:18-20

[41] Woo DS, Kim YG, Kim KW, Cho YK. Design of quasi-Yagi antennas using an ultra-wideband balun. *Microwave and Optical Technology Letters*. 2008;50(8):2068-2071

[42] Ta SX, Kim B, Choo H, Park I. Slot-line-fed quasi-Yagi antenna. In: *Proc. Int. Symp. on Antennas Propagation and EM Theory*, Dec. Guangzhou; 2010. pp. 307-310

[43] Nguyen PT, Abbosh A, Crozier S. Wideband quasi-Yagi antenna with tapered driver. In: *Proc. Asia-Pacific Conf. on Antennas and Propagation*, Singapore. 2012. pp. 138-139

[44] Jiang K, Guo QG, Huang KM. Design of a wideband quasi-Yagi microstrip antenna with bowtie active elements. In: *Proc. Int. Conf. on Microwave and Millimeter Wave Technology (ICMMT)*. 2010. pp. 1122-1124

[45] Wu J, Zhao Z, Nie Z, Liu Q-H. A broadband unidirectional antenna based on closely spaced loading method. *IEEE Transactions on Antennas and Propagation*. 2013;61:109-116

[46] Matthias J, Ammann M, McEvoy P. UWB Vivaldi antenna based on aspline geometry with frequency band-notch. In: *Proc. IEEE Antennas Propag. Soc. Int. Symp. San Diego, CA USA*; 2008. pp. 1-4

[47] Ta SX, Kim B, Choo H, Park I. Wideband quasi-Yagi antenna fed by microstrip-to-slot line transition. *Microwave and Optical Technology Letters*. 2012;54(1):150-153

[48] Zanzoni A, Montecchi-Palazzi L, Quondam MX. *Mint: A molecular interaction database*